THE JOURNAL OF PHYSICAL CHEMISTRY C
A JOURNAL OF THE AMERICAN CHEMICAL SOCIETY

pubs.acs.org/JPCC

Article

# Phase Transitions of $BiVO_4$ under High Pressure and High Temperature

Josu Sánchez-Martín, Daniel Errandonea,* Julio Pellicer-Porres, David Vázquez-Socorro, Domingo Martínez-García, S. Nagabhusan Achary, and Catalin Popescu

Cite This: *J. Phys. Chem. C* 2022, 126, 7755−7763

Read Online

ACCESS | Metrics & More | Article Recommendations

**ABSTRACT:** We have studied the occurrence of phase transitions in two polymorphs of $BiVO_4$ under high-pressure and high-temperature conditions by means of X-ray diffraction measurements. The fergusonite polymorph undergoes a phase transition at 1.5(1) GPa and room temperature into a tetragonal scheelite-type structure. The same transition takes place at 523(1) K and ambient pressure. A second phase transition takes place at room temperature under compression at 16(1) GPa. The transition is from the tetragonal scheelite structure to a monoclinic structure (space group $P2_1/c$). All observed phase transitions are reversible. The zircon polymorph counterpart also transforms under compression into the scheelite-type structure. In this case, the transitions take place at 4.3(1) GPa and room temperature and at 653(1) K and ambient pressure. The zircon−scheelite transition is nonreversible. The experiments support that the fergusonite−scheelite transformation is a second-order transition and that the zircon−scheelite transformation is a first-order transition. Finally, we have also determined the compressibility and the thermal expansion of the fergusonite, scheelite, and zircon phases.

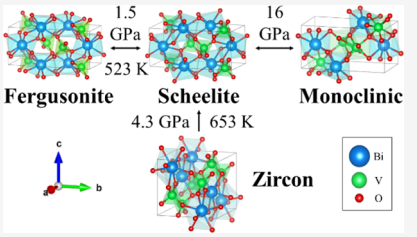




## 1. INTRODUCTION

Bismuth vanadate ($BiVO_4$) has recently been under focus for its potential use in photocatalysis[1] for hydrogen production via water splitting.[2,3] It has also attracted attention for decades because of its complex structural phase diagram,[4] tunable properties when being doped,[5−7] its rich polymorphism depending on preparation conditions, and external thermodynamic parameters.[8] The high-pressure (HP) and high-temperature (HT) behavior of $BiVO_4$ has attracted attention for nearly half a century.[4,9] This compound is known to crystallize either into the stable monoclinic fergusonite-type polymorph (space group $I2/a$)[10] or in the metastable tetragonal zircon-type polymorph (space group $I4_1/amd$).[11] Furthermore, a third polymorph occurs in nature as a mineral with an orthorhombic structure known as Pucherite (space group $Pnca$[12]). At 523(1) K and ambient pressure, fergusonite-type $BiVO_4$ undergoes a transition to a tetragonal scheelite-type polymorph (space group $I4_1/a$).[9,13] Hydrostatic pressure reduces the transition temperature[14,15] and makes it possible to induce the fergusonite−scheelite transition by compression at room temperature (RT).[4] It is known that the zircon-type polymorph also transforms under compression into the scheelite-type polymorph.[16,17] The structural stability of the scheelite-type phase has been also studied.[6,17] There is an agreement in the fact that this polymorph suffers a phase transition near 20 GPa. However, two different monoclinic structures have been proposed for the post-scheelite (PS) phase.[6,17] This discrepancy needs to be clarified.[18] In addition, the PS structures reported for $BiVO_4$ are different from the PS structure known for other ternary oxides, for example, $BaWO_4$,[19] $HoNbO_4$,[20] $EuNbO_4$,[21] and $GdVO_4$.[22] This fact also calls for further studies to fully understand the HP and HT behavior of $BiVO_4$ and such a family of technologically important compounds.

In this work, we have studied the HP and HT structural properties of $BiVO_4$ up to 26.4(1) GPa and 873(1) K. Our results allowed us to determine the room-temperature pressure−volume equation of state (EOS) of three polymorphs, namely, zircon, scheelite, and fergusonite types. Additionally, we have also determined the isothermal compressibility tensor and the thermal expansion coefficients for the fergusonite-type polymorph.

## 2. EXPERIMENTAL DETAILS

Polycrystalline fergusonite-type $BiVO_4$ was purchased from Alfa-Aesar (99.9% purity). Nanometric powder of zircon-type $BiVO_4$ was synthesized by a precipitation method from the acidic aqueous solution of $Bi(NO_3)_3$ and $NH_4VO_3$ at RT.[23] The composition and crystal structure of the samples was

**Received:** February 18, 2022
**Revised:** April 8, 2022
**Published:** April 21, 2022

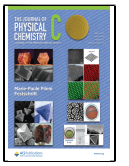

**Table 1. Label and Details of the Experiments**

| name | type | initial sample | PTM | P scale | $\lambda$ (Å) | $P/T$ max. |
|---|---|---|---|---|---|---|
| HP1 | HP | fergusonite | MEW | Cu | 0.4246 | 17.7 GPa |
| HP2 | HP | fergusonite | Ne | ruby | 0.4246 | 26.4 GPa |
| HP3 | HP | fergusonite | N | ruby | 0.4246 | 18.5 GPa |
| HP4 | HP | zircon | MEW | ruby | 0.4246 | 25.6 GPa |
| HP5 | HP | zircon | silicon oil | ruby | 0.3738 | 4.1 GPa |
| HT1 | HT | fergusonite | | | 1.54059 | 873 K |
| HT2 | HT | zircon | | | 1.54059 | 873 K |
| HPHT | HP-HT | fergusonite | MEW | $SrB_4O_7:Sm^{2+}$ | 0.4246 | 403 K |

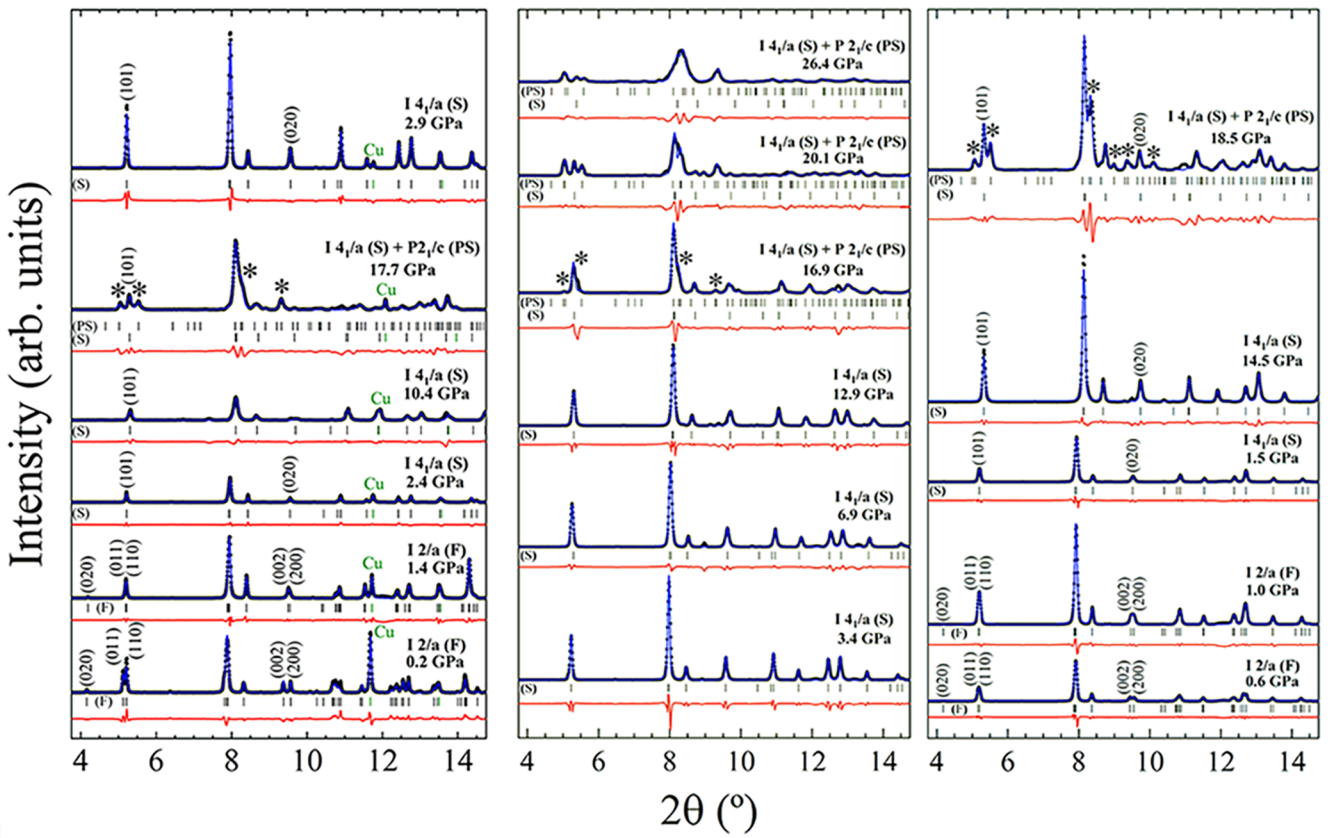


**Figure 1.** XRD patterns at selected pressures starting from the fergusonite polymorph (F) for experiments HP1 (a), HP2 (b), and HP3 (c). Experiments are shown with black circles, and the Le Bail fits and their residuals are shown with solid (blue and red, respectively) lines. Ticks indicate the positions of the Bragg peaks for the different phases. The index of the peaks mentioned in the text is shown. The asterisks mark fingerprints of the onset of the PS phase. (a) Positions of Cu peaks are indicated with green ticks, and the one used for pressure determination is labeled as Cu. A pattern measured under decompression at 2.9(1) GPa for the scheelite (S) phase is shown in the top trace.

confirmed by ambient conditions powder X-ray diffraction (XRD). HP studies up to 26.4(1) GPa were carried out using a membrane-type diamond-anvil cell. As pressure-transmitting media (PTM) we used either neon (Ne), nitrogen (N), a 16:3:1 methanol−ethanol−water mixture (MEW), or silicon oil. These different PTM remains quasi-hydrostatic up to different maximum pressures.[24] Thus, nonhydrostatic effects could potentially influence the observed results and the $P-T$ phase diagram; especially at pressures beyond 10 GPa.[24] In the next section, we will show that our experiments suggest that in $BiVO_4$, within the pressure range covered by our studies, compressibilities are more affected by nonhydrostatic effects than transition pressures. The pressure was determined using either the ruby fluorescence method[25] or the EOS of copper (Cu),[26] both with a precision of ±0.1 GPa. We performed HP powder XRD measurements at the MSPD beamline of the ALBA synchrotron using a monochromatic beam of wavelength 0.4246 Å. The beam was focused down to a 20 $\mu$m × 20 $\mu$m full width at half maximum (fwhm) spot. A Rayonix charge-coupled device detector was used to collect XRD patterns, with a sample detector distance of 240 mm. HP−HT synchrotron experiments were carried out employing external resistive heating. The temperature was measured using a K-type thermocouple in close contact with the diamonds. In this setup, the pressure was determined using the fluorescence line of $SrB_4O_7:Sm^{2+}$.[27] We also performed XRD measurements at the PSICHÉ beamline of the SOLEIL synchrotron with a wavelength of 0.3738 Å. A MAR detector was used to collect XRD patterns, with a sample detector distance of 735 mm. HT powder XRD measurements up to 873(1) K were carried out at Servicio Central de Soporte a la Investigación Experimental (SCSIE) from the University of Valencia using a Bruker D8


https://doi.org/10.1021/acs.jpcc.2c01184
J. Phys. Chem. C 2022, 126, 7755−7763

AVANCE A25 powder diffractometer with a Bragg−Brentano geometry and Cu $K_{\alpha 1}$ radiation ($\lambda$ = 1.54059 Å). The sample was heated under vacuum ($10^{-4}$ mbar) using an Anton Paar chamber HTK1200N, and the temperature was determined with an S-type thermocouple with a precision of ±1 K. More details of each experiment can be found in Table 1. The structural analysis was performed with PowderCell[28] and GSAS-II.[29]

## 3. RESULTS AND DISCUSSION

**3.1. X-ray Diffraction Measurements under HP and HT.** We have performed three different HP powder XRD experiments starting with the fergusonite structure. Despite the different PTM used, in all of them, we have found a qualitatively similar behavior. To illustrate it, in Figure 1, we show a selection of XRD patterns collected in the experiments labeled as HP1 (Figure 1a), HP2 (Figure 1b), and HP3 (Figure 1c). The patterns at pressures smaller than 1.5(1) GPa can be assigned to the fergusonite structure. At 1.5(1) GPa, there are changes that are considered fingerprints for the fergusonite-scheelite transition.[4,16] The most notorious facts are the vanishing of the (020) peak of fergusonite and the merging of two couples of fergusonite peaks [(011) with (110) and (002) with (200)] into two single peaks [(101) and (020) peaks of scheelite, respectively)] due to the symmetry increase at the transition. This conclusion is supported by a Le Bail analysis shown in Figure 1. From 1.5(1) to 16(1) GPa, the XRD patterns can be assigned to the scheelite structure.

Beyond 16(1) GPa, we detected changes in XRD patterns indicating a second structural phase transition. The most relevant changes (highlighted with asterisks in Figure 1) are the appearance of two extra peaks on the left and right side of the (101) peak of scheelite, the broadening of the strong peak at $2\theta \approx 8°$, and the emergence of additional peaks at higher angles. To try to explain the XRD of the PS phase, we have considered the structures previously reported in the literature, that is, different monoclinic structures described by space groups $C2/c$[17] and $P2_1/n$.[6] However, none of them (alone or in coexistence with scheelite) can account for all observed peaks. Then, we tried several PS structures previously reported for related ternary oxides that have the fergusonite structure at ambient pressure.[19−21] The best Le Bail fit was obtained with the monoclinic structure described by the space group $P2_1/c$ reported by Garg et al.[20] for $HoNbO_4$. Assuming this structure in coexistence with scheelite we can explain all observed peaks after the second phase transition. This suggests that the monoclinic postfergusonite structure of $HoNbO_4$ is a reasonable candidate for the crystal structure of PS $BiVO_4$. From 16(1) to 26.4(1) GPa, the PS structure coexists with the scheelite one. Under decompression up to 2.9(1) GPa, we have recovered the scheelite structure. The reversibility of the fergusonite−scheelite phase transition is in accordance with the character of the ferroelastic transition,[4,9] which is of the second order. In fact, it is thoroughly checked in the HP−HT experiment.

Experiment HP4 starts from the zircon polymorph ($I4_1/amd$). A selection of XRD patterns from this experiment is shown in Figure 2. The patterns up to 4.3(1) GPa can be undoubtedly assigned to the zircon structure. This transition pressure is in good agreement with the literature, where it was found between 3.7[16] and 5 GPa.[17] From 4.3(1) to 6.2(1) GPa, we observed the coexistence of the zircon phase with an HP scheelite-type polymorph. From 7.6(1) to 25.6(1) GPa, the patterns could be fitted with the scheelite structure. However, a detailed analysis of the fwhm of (101) reflection shows an increase at 16(1) GPa. This fact could be related to nonhydrostatic effects[24] but could also suggest a phase transition to the PS phase, as happens in the experiments made starting from the fergusonite polymorph. The PS peaks marked with asterisks in Figure 1 are not as appreciable in Figure 2 due to the broadening of the peaks. To further clarify this point, we show in Figure 2 two different Le Bail fits at 25.6(1) GPa considering or not considering the PS contribution. The second option explains better the experiments. Cheng et al.[17] in their study of zircon-type $BiVO_4$ reported the onset of the second phase transition at 25.4 GPa, a pressure higher than the present transition pressure. The differences could be related to the different PTM used in the experiments.[30] Under decompression at 0.8(1) GPa, we recover the fergusonite-type $BiVO_4$ as the stable polymorph.

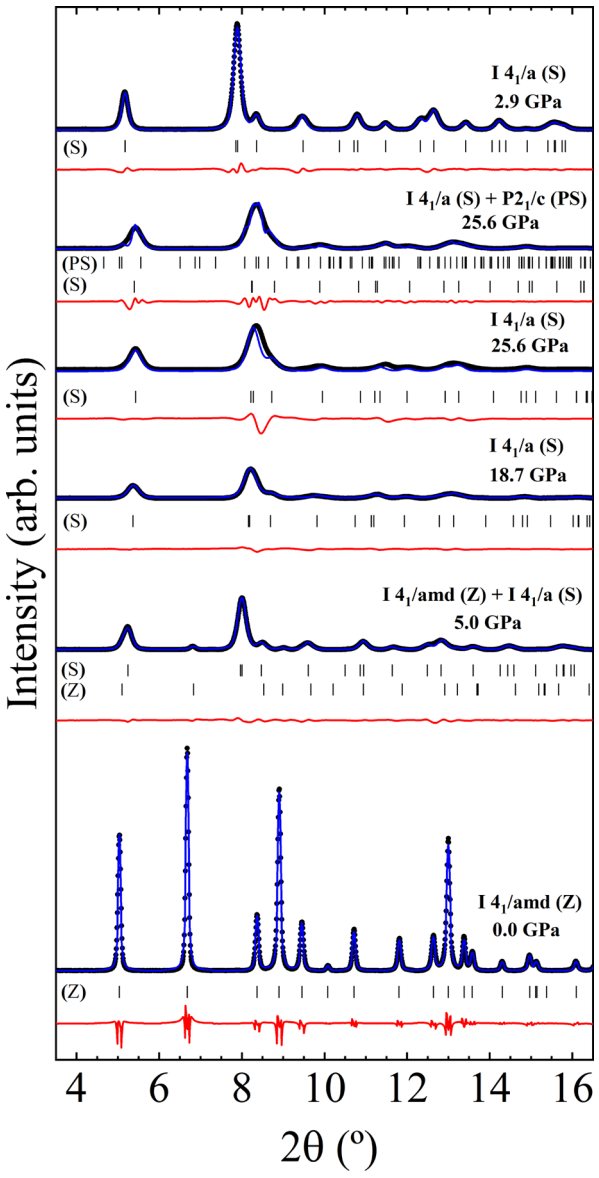


**Figure 2.** XRD patterns at selected pressures starting from the zircon polymorph for experiment HP4. Experiments are shown with black circles. Le Bail fits and residuals are shown with blue and red lines, respectively. Ticks indicate the positions of the Bragg peaks for the phase indicated on the left of the figure.



https://doi.org/10.1021/acs.jpcc.2c01184
J. Phys. Chem. C 2022, 126, 7755−7763

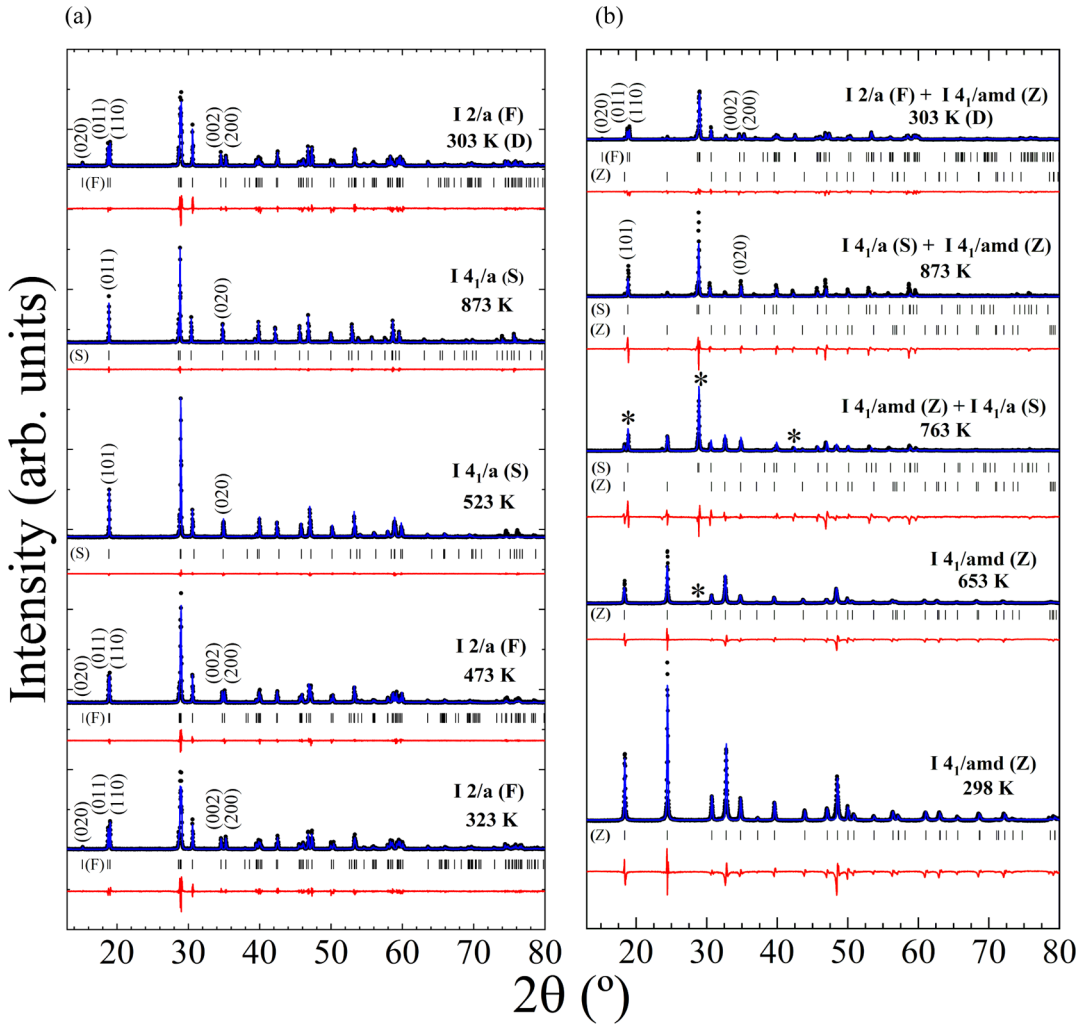


**Figure 3.** XRD patterns at selected temperatures starting from the fergusonite polymorph (F) for experiments HT1 (a) and HT2 (b). Experiments are shown with black circles, and the Le Bail fits and their residuals are shown with solid (blue and red, respectively) lines. Ticks indicate the positions of the Bragg peaks for the different phases. The index of the peaks mentioned in the text is shown. A pattern measured cooling until RT (D) is shown in the top trace. (b) Asterisks mark fingerprints of the onset of the scheelite (S) phase.

The XRD patterns corresponding to the HP5 experiment are very similar to those shown in Figure 2, and for the sake of briefness, we do not reproduce them here.

We have also performed XRD measurements for $BiVO_4$ as a function of temperature at ambient pressure in experiments HT1 (Figure 3a) and HT2 (Figure 3b). The HT1 experiment starts from the fergusonite-type polymorph. From 323(1) to 523(1) K, the sample remains in its initial structure. We could precisely determine the temperature of the phase transition into the scheelite structure measuring at temperature steps of 10(1) K and looking for the fingerprint changes recognition described for the analogous HP transition. This phase transition was observed in a previous Raman experiment[16] at 528(5) K. From 523(1) to 873(1) K, $BiVO_4$ remains stable as a scheelite polymorph. When cooling down to RT, we recognized a fergusonite-type pattern, confirming the reversibility of the fergusonite−scheelite phase transition.

We will comment now on the HT XRD measurements made in the zircon-type polymorph (experiment HT2, Figure 3b). We have found that from 298(1) to 643(1) K, the sample remains in its initial zircon structure. At 653(1) K, we started to recognize extra peaks that could be assigned to the scheelite structure. This transition temperature is close to the 690(10) K reported in the Raman experiment.[16] Both phases coexist up to 873(1) K, the highest temperature covered by experiment HT2. As the temperature was quenched from 873(1) to 303(1) K, the XRD patterns still had contributions of the zircon structure, but the scheelite structure shifted to the expected fergusonite-type polymorph. We conclude that we found a partial transformation from zircon to scheelite with the onset of the transition at 653(1) K. Because the transition is nonreversible, the fraction of the sample transformed into scheelite returns to the stable fergusonite structure coexisting with the remaining zircon-type sample after the sample is cooled down to RT.

We have also performed an XRD experiment applying simultaneously HP and HT, labeled as HPHT. In these experiments, we observed only the scheelite and fergusonite phases. In Figure 4a, we provide XRD patterns and LeBail fits for selected pressures at 398(1) K. In Figure 4b, we represent the $P-T$ path followed in this experiment and a schematic representation of the phase diagram. In the diagram, the $P-T$ points corresponding to fergusonite and scheelite are represented in blue and red, respectively. The fergusonite−scheelite phase boundary can be represented by a linear relation as $T_{F-S}$ (K) = −141(12) × $P$ (GPa) + 523(2), in


https://doi.org/10.1021/acs.jpcc.2c01184
J. Phys. Chem. C 2022, 126, 7755−7763

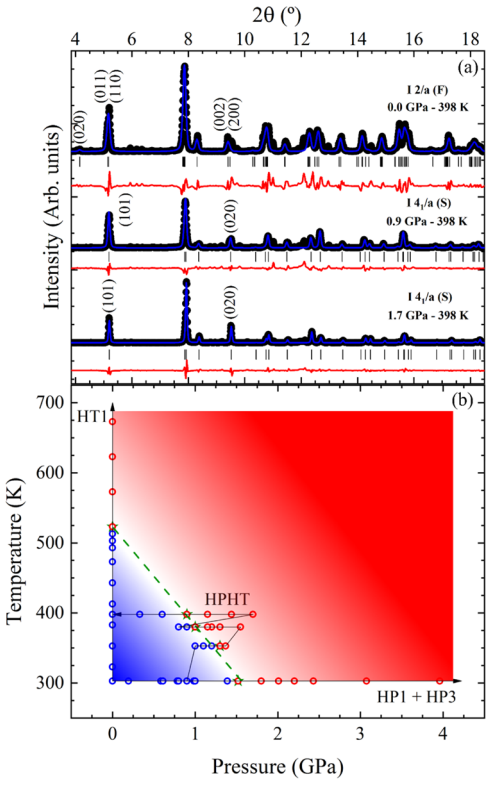


**Figure 4.** (a) Selected XRD patterns for the HPHT experiment following the 398(1) K isotherm. Experiments are shown with black circles, and the Le Bail fits and their residuals are shown with solid (blue and red, respectively) lines. Ticks indicate the positions of the Bragg peaks for the different phases. The index of the peaks mentioned in the text is shown. (b) Phase diagram built with results of experiments HP1, HP3, HT1, and HPHT. The $P-T$ path followed in the experiments is shown with arrows. The fergusonite-type and scheelite-type polymorphs are represented with blue and red circumferences, respectively. The dashed green line is a linear fit ($R^2$ = 0.991) of the data points identified as scheelite right next to data points identified as fergusonite (green stars).

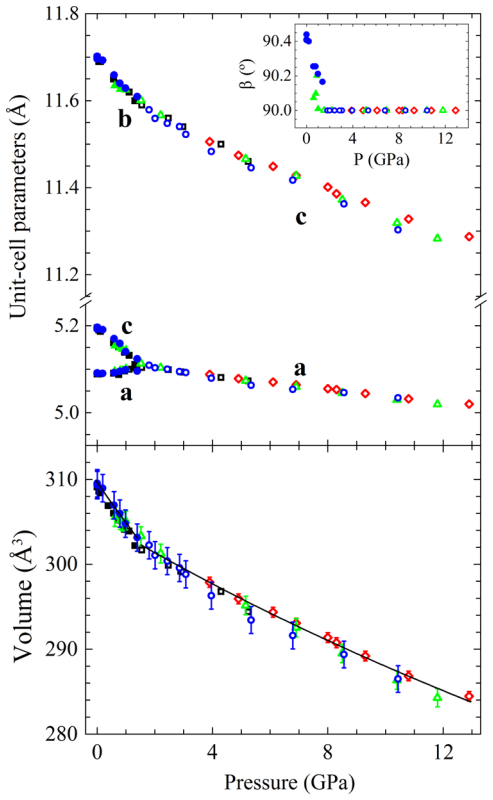


**Figure 5.** Pressure dependence beginning with the fergusonite phase of the unit-cell parameters (top), volume (bottom), and beta angle (inset) for the experiments HP1 (blue circles), HP2 (red diamonds), and HP3 (green triangles), and results reported by Hazen and Mariathasan.[4] are also shown (black squares). Filled and empty symbols represent the fergusonite and scheelite phases, respectively. The calculated EOS (see text) are shown with solid lines.

agreement with literature.[4,16] This boundary is represented by a green dashed line in Figure 4. The negative slope of the phase boundary means that according to the Clausius–Clapeyron relation the entropy of scheelite is higher than the entropy of fergusonite. Moreover, our HPHT experiment shows the lack of hysteresis characteristic of a second-order phase transition.

**3.2. Compressibility and Thermal Expansion.** From the analysis of HP XRD patterns, we have extracted the unit cell parameters and volume of different structures as a function of pressure. These results are reported in Figure 5 for the experiments beginning with the fergusonite phase HP1, HP2, and HP3. For the sake of accuracy, we only include results for the pressure points where there is no phase coexistence ($P$ < 15 GPa) in the three experiments. The fergusonite–scheelite phase transformation has no change in the unit-cell volume, which agrees with the second-order nature of the transition. The unit-cell parameters of all three experiments evolve under pressure in agreement with the behavior reported by Hazen and Mariathasan.[4]

Results for the pressure dependence of unit-cell parameters and volume for the experiments that start from the zircon polymorph HP4 and HP5 are shown in Figure 6. HP5 is represented up to the first phase transition. The scattering of results for the c parameter in the HP4 experiment beyond 4 GPa is probably related to the coexistence of the zircon and scheelite phases, which makes indexation less accurate. The zircon–scheelite phase transformation has a collapse of the volume of 7.4%, which marks that this is a first-order phase transition. We have also noticed a systematic offset in the results obtained upon decompression. This fact could be related to hysteresis effects on the PTM when releasing pressure, which is occasionally observed using MEW when the solidification pressure, 10.5 GPa, is exceeded.[24]

We will comment now on the changes induced by pressure in the unit-cell parameters of different phases. In the case of the monoclinic fergusonite structure, the compressibility tensor is not diagonal in the reference system defined by the lattice parameters. Thus, we described the compressibility of the fergusonite structure by means of the eigenvalues and eigenvectors of the isothermal compressibility tensor,[31] which are summarized in Table 2 for the pressures indicated. They have been obtained using PASCal.[32] For the tetragonal scheelite (HP2) and zircon (HP4) structures, we directly calculate the axial compressibility of the $a$- and $c$-axis as $\kappa_a = \frac{1}{a}\left(\frac{\partial a}{\partial P}\right)_T$ and $\kappa_c = \frac{1}{c}\left(\frac{\partial c}{\partial P}\right)_T$, respectively. From Table 2, it can be seen that the compression of the three structures is anisotropic. In the fergusonite structure, the most compressible direction ($e_{v3}$) is in the plane perpendicular to the unique $b$-axis and making an angle of 8° with the $c$-axis. In addition, in the same plane, along the direction $e_{v1}$ (which is perpendicular


https://doi.org/10.1021/acs.jpcc.2c01184
J. Phys. Chem. C 2022, 126, 7755–7763

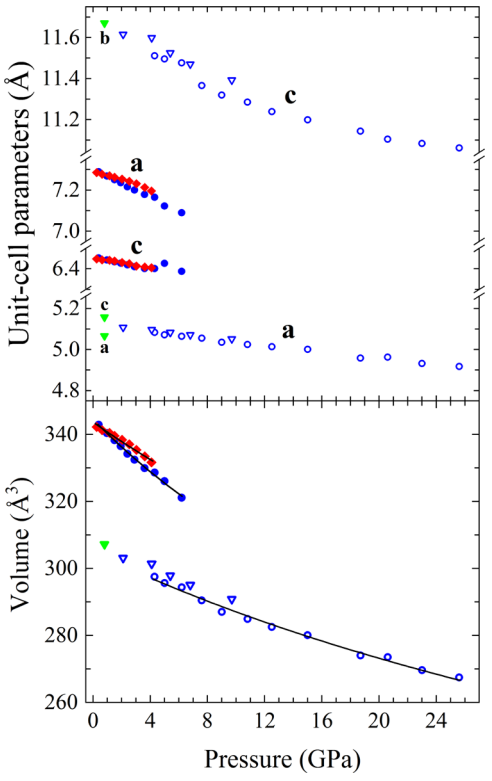


**Figure 6.** Pressure dependence beginning with the zircon polymorph of the unit-cell parameters (up) and volume (down) for HP4 and HP5 experiments. Solid and empty blue symbols stand for the HP4 zircon and scheelite phases, respectively. Circles represent compression, while triangles mark decompression. Green triangles represent a HP4 fergusonite structure. Red diamonds stand for the HP5 zircon phase. The fitted EOS is shown with a solid line.

to $e_{v3}$), the fergusonite structure undergoes an expansion as pressure increases. In scheelite, we found that the *c*-axis is 44% more compressible than the *a*-axis. In zircon, the *c*-axis is 53% less compressible than the *a*-axis. These results agree with results reported for the same phases in other vanadates.[8,33] The anisotropic behavior is related to the larger compressibility of $BiO_8$ dodecahedral units with respect to $VO_4$ tetrahedral units and the modes of linking these polyhedra in the respective crystal structures.

Regarding the pressure dependence of the unit-cell volume of different structures, we have analyzed it using a second-order Birch–Murnaghan EOS[34] ($K_0' = 4$). The order of the EOS was determined from the Eulerian strain-normalized pressure plot of the data.[35] The obtained values for the ambient-pressure volume ($V_0$) and bulk modulus ($K_0$) are summarized in Table 3. They have been fitted using EosFit7.[36] The corresponding EOSs are plotted in Figures 5 and 5. In Table 3, our EOS parameters are compared with the results of previous experiments[4,17] and calculations.[37] The fit to the zircon data yielded two incompatible values for the bulk modulus. In fact, the two volume curves represented with solid symbols in Figure 6, lower panel, clearly have different slopes. We suggest that the hydrostaticity of the PTM is affecting the results. In the HP4 experiment, we used MEW, a fully hydrostatic PTM in this pressure range,[24] and in the HP5 experiment, silicon oil was used instead, which starts to lose hydrostaticity at 2.5 GPa.[24] We then consider the HP4 experiment more reliable.

The results obtained from fergusonite- and zircon-type $BiVO_4$ indicate that this compound is one of the most compressible orthovanadates. The range of $K_0$ values reported for the $AVO_4$ family varies from 110 to 188 GPa for fergusonite-type polymorphs and from 93 to 160 GPa for zircon-type ones.[8]

The results obtained for the scheelite structure in the experiment starting from fergusonite are fully consistent with those obtained in the experiment starting from zircon. They also agree with the results reported by Hazen and Mariathasan.[4] This agreement and the quasi-hydrostatic conditions of our experiments suggest that the bulk modulus of scheelite-type $BiVO_4$ has been underestimated by the experiments of Cheng et al.[17] and the calculations of Farid Ul Islam et al.[37] In the fergusonite structure, there is again an excellent agreement between our results and the results reported by Hazen and Mariathasan.[4] In this case, computer simulations[37] largely overestimate the bulk modulus. For the zircon structure, our bulk modulus is around 20–30% smaller than the results reported by Cheng et al.[17] and Farid Ul Islam et al.[37] However, we are confident in our bulk modulus for several reasons. First, calculations do not provide the correct bulk modulus neither for fergusonite nor for scheelite. Second, Cheng et al.[17] reported a similar bulk modulus for zircon and scheelite, which is not expected given the large volume collapse at the zircon-scheelite transition.[33] We think the results of Cheng et al.[17] could be hindered by three reasons: first, the scarcity of data points measured for the zircon phase; second, the fact that two of the four data points were obtained from the coexistence of zircon and scheelite; finally, the use of argon as a PTM, which becomes solid at 2 GPa[24,38] (similarly to what is observed in the HP5 experiment with silicon oil). In fact, probably because of the last reason, the transition pressure reported by Cheng et al.[2,17] in GPa (i.e., it agrees with the solidification pressure of argon) is also lower than our transition pressure.

From the XRD measurements of experiments HT1 and HT2, we have calculated the unit-cell parameters and volume as a function of temperature for different phases. The results are plotted in Figures 7 and 8, respectively. We can see that the fergusonite-scheelite phase transition in Figure 7 has no volume change, as it was observed under HP in Figure 5. In Figure 8 we have plotted the lattice parameters for the zircon structure up to 743(1) K. We focused on this structure to obtain its thermal expansion. Due to the phase coexistence of zircon in scheelite in experiment HT2, for the sake of accuracy,

**Table 2. Eigenvalues, $\lambda_i$ ($GPa^{-1}$), and Eigenvectors, $e_{vi}$, for the Isothermal Compressibility Tensor of the Fergusonite Phase and Axial Compressibilities for Zircon and Scheelite**

| fergusonite-type (0.6(1) GPa) | | scheelite-type (3.9(1) GPa) | zircon-type (0.4(1) GPa) |
|---|---|---|---|
| $\lambda_1 = -1.3(9)\ 10^{-3}$ | $e_{v1} = (0.99, 0, 0.16)$ | $\kappa_a = 1.6(2)\ 10^{-3}\ GPa^{-1}$ | $\kappa_a = 4.7(3)\ 10^{-3}\ GPa^{-1}$ |
| $\lambda_2 = 5.9(9)\ 10^{-3}$ | $e_{v2} = (0, 1, 0)$ | | |
| $\lambda_3 = 10.4(1.5)\ 10^{-3}$ | $e_{v3} = (-0.16, 0, 0.99)$ | $\kappa_c = 2.3(4)\ 10^{-3}\ GPa^{-1}$ | $\kappa_c = 2.5(4)\ 10^{-3}\ GPa^{-1}$ |



https://doi.org/10.1021/acs.jpcc.2c01184
J. Phys. Chem. C 2022, 126, 7755–7763

**Table 3. EOS Parameters from This Work and the Literature**[a]

| | this work | | Hazen and Mariathasan[4] | | Cheng et al.[17] | | Farid Ul Islam et al.[37] | |
|---|---|---|---|---|---|---|---|---|
| phase | $V_0$ (Å) | $K_0$ (GPa) | $V_0$ (Å) | $K_0$ (GPa) | $V_0$ (Å) | $K_0$ (GPa) | $V_0$ (Å) | $K_0$ (GPa) |
| fergusonite | 309.7 (0.3) | 62(4) | 309.1 | 64.9 | | | 302 | 111.5 |
| scheelite (F) | 305(2) | 148(6) | 304.8 | 144.9 | | | 309 | 132.4 |
| scheelite (Z) | 305(1) | 145(5) | | | 306.1 | 116.3 | | |
| zircon (HP4) | 344.5(0.4) | 78(3) | | | 342.6 | 101.1 | 349 | 112.5 |
| zircon (HP5) | 344(3) | 113(17) | | | | | | |

[a]All of them have been obtained using a 2nd order Birch−Murnaghan EOS ($K_0' = 4$). Scheelite (F) and Scheelite (Z) are results from experiments starting from fergusonite and zircon, respectively. The results of Farid Ul Islam et al. are from calculations.

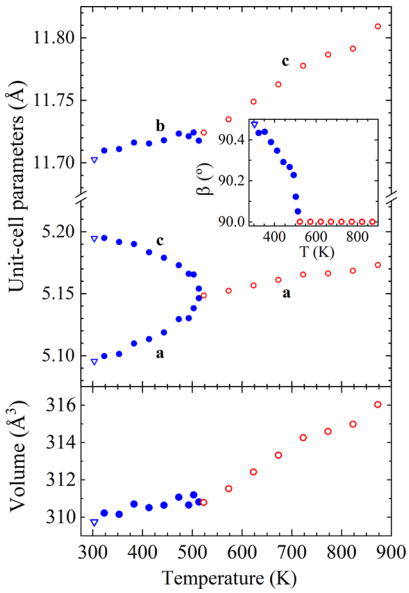


**Figure 7.** Temperature dependence of the unit-cell parameters and volume for the experiment HT1. Blue solid and red empty symbols stand for the fergusonite and scheelite phases, respectively. The blue triangle symbols stand for the data taken going back to RT. The evolution of the fergusonite $\beta$ angle is displayed in the inset.

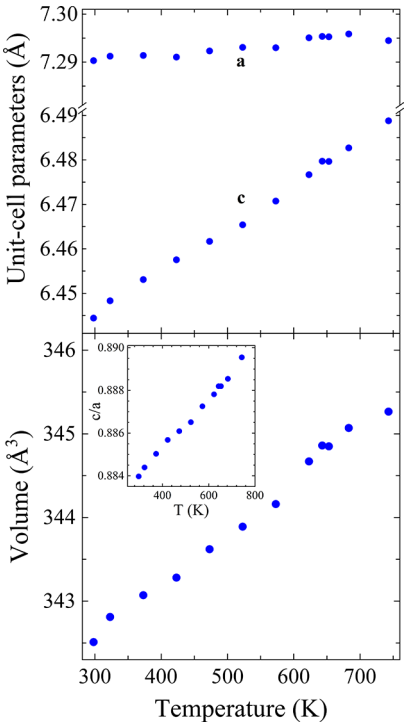


**Figure 8.** Temperature dependence of the unit-cell parameters and volume for the zircon structure in experiment HT2. The $c/a$ ratio is shown in the inset.

the thermal expansion of scheelite was determined from experiment HT1.

In order to obtain the thermal expansion of the three phases involved in both HT experiments, we followed an analogous procedure to compressibility. For the monoclinic fergusonite structure, we describe the thermal expansion by means of the eigenvalues and eigenvectors of the isobaric thermal expansion tensor.[31] The temperature region used is from 303(1) to 443(1) K. They have also been obtained using PASCal.[32] For the tetragonal structures, we simply used the axial thermal expansions of the $a$- and $c$-axis of $\alpha_a = \frac{1}{a}\left(\frac{\partial a}{\partial T}\right)_P$ and $\alpha_c = \frac{1}{c}\left(\frac{\partial c}{\partial T}\right)_P$, respectively. The regions used for the linear fits are from 523(1) to 723(1) K for scheelite and from 298(1) to 643(1) K for zircon. We summarized all the results in Table 4 for the temperatures indicated. The thermal expansion of the three structures is anisotropic. The main axes for the thermal expansion and hydrostatic compression in the fergusonite structure are the same. In the scheelite structure, we have found that the ratio axial thermal expansion is similar to that of axial compressibility ($\alpha_c/\alpha_a \sim \kappa_c/\kappa_a$). In the zircon structure $\alpha_c > \alpha_a$. This can be clearly seen in the inset of Figure 8 where we represent the $c/a$ ration as a function of temperature. In scheelite, the difference between thermal expansion coefficients is much smaller. A final interesting fact we would like to comment on is that the $b$-axis of fergusonite corresponds to the $c$-axis of scheelite. However, the $b$-axis of fergusonite has the lowest thermal expansion coefficient, while the $c$-axis of scheelite has the largest thermal coefficient. This could be related to the reorientation of $BiO_8$ and $VO_4$ polyhedra at the transition, that is, the transition occurs simply by tilting of the polyhedra.

To conclude, we have used the Landau theory to support the second-order nature of the fergusonite−scheelite phase transition. We have used two approaches. The first one is based on the calculation of the spontaneous strain ($\varepsilon_s$) of the fergusonite structure related to the scheelite following an analogous procedure to that used to study $Eu_{0.1}Bi_{0.9}VO_4$ under HP.[6] In order to calculate $\varepsilon_s$, we have used the definition given by Aizu.[15,39] In the second approach, we have analyzed the temperature dependence of the deviation of the $\beta$ angle from 90° ($\beta$—90°), following the approach used by Arulnesan et al. to study the fergusonite-scheelite transition in niobates.[40] According to the Landau theory, both $\varepsilon_s$ and $\beta$—90° should be proportional to $\sqrt{|T - T_{Trans}|}$, where $T$ is the temperature and



https://doi.org/10.1021/acs.jpcc.2c01184
J. Phys. Chem. C 2022, 126, 7755−7763

Table 4. Eigenvalues, $\lambda_i$ ($K^{-1}$), and Eigenvectors, $e_{vi}$, for the Isobaric Thermal Expansion Tensor of the Fergusonite Phase and Axial Thermal Expansions for Zircon and Scheelite

| fergusonite-type (303(1) K) | | scheelite-type (523(1) K) | zircon-type (298(1) K) |
|---|---|---|---|
| $\lambda_1$ = 74(8) $10^{-6}$ | $e_{v1}$ = (0.98, 0, 0.20) | $\alpha_a$ = 17.6(2) $10^{-6}$ $K^{-1}$ | $\alpha_a$ = 1.8(7) $10^{-6}$ $K^{-1}$ |
| $\lambda_2$ = 6.7(1.2) $10^{-6}$ | $e_{v2}$ = (0, 1, 0) | | |
| $\lambda_3$ = −64(8) $10^{-6}$ | $e_{v3}$ = (0.20, 0, −0.98) | $\alpha_c$ = 23.1(3) $10^{-6}$ $K^{-1}$ | $\alpha_c$ = 15.0(4) $10^{-6}$ $K^{-1}$ |

$T_{Trans}$ the transition temperature.[12,38] In our case, we know that $T_{Trans}$ = 523(1) K. In Figure 9, we show $\varepsilon_s$ and $\beta$—90° versus temperature and fits using functions of the form $\varepsilon_s = A(|T - T_{Trans}|)^n$ and $\beta$—90° = $A(|T - T_{Trans}|)^n$. In the first case, the best fit is obtained for $n$ = 0.56(7). In the second case, it is obtained for $n$ = 0.48(11). Both results are consistent with $n$ = 0.5, the value expected for a second-order transition. Thus, we conclude that the HT fergusonite−scheelite transition of $BiVO_4$ is a proper second-order transformation.

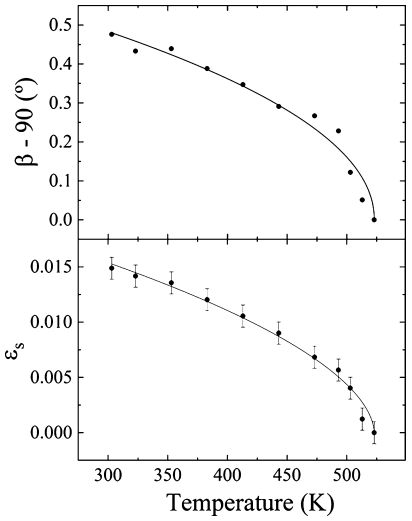


**Figure 9.** $\beta$—90 and spontaneous strain $\varepsilon_s$ as a function of temperature. Results obtained from experiment HT1. In the plot of $\beta$—90, errors are smaller than symbols. The solid lines represent the fits described in the text.

## 4. CONCLUSIONS

HP and HT angle dispersive powder XRD experiments were performed in $BiVO_4$ up to 26.4(1) GPa and 873(1) K. The reversible fergusonite−scheelite transition has been characterized, the $P$−$T$ phase diagram was determined, and the second-order nature of the transition was verified. The irreversible zircon−scheelite transition has been found at 4.3(1) GPa and RT and 653(1) K and at ambient pressure. A second phase transition scheelite-PS has been found at 16(1) GPa. This transition is reversible. We propose for the PS phase a monoclinic structure belonging to the space group $P2_1/c$. The pressure dependence of the unit-cell parameters and the equations of state of different phases are reported. The compressibility and the thermal expansions of the same phases have been calculated.

## AUTHOR INFORMATION


### Corresponding Author

**Daniel Errandonea** − *Departamento de Física Aplicada-ICMUV, Universidad de Valencia, 46100 Valencia, Spain;* orcid.org/0000-0003-0189-4221; Email: daniel.errandonea@uv.es

### Authors

**Josu Sánchez-Martín** − *Departamento de Física Aplicada-ICMUV, Universidad de Valencia, 46100 Valencia, Spain;* orcid.org/0000-0003-0241-0217

**Julio Pellicer-Porres** − *Departamento de Física Aplicada-ICMUV, Universidad de Valencia, 46100 Valencia, Spain*

**David Vázquez-Socorro** − *Departamento de Física Aplicada-ICMUV, Universidad de Valencia, 46100 Valencia, Spain*

**Domingo Martínez-García** − *Departamento de Física Aplicada-ICMUV, Universidad de Valencia, 46100 Valencia, Spain*

**S. Nagabhusan Achary** − *Chemistry Division, Bhabha Atomic Research Centre, Mumbai 400085, India;* orcid.org/0000-0002-2103-1063

**Catalin Popescu** − *CELLS-ALBA Synchrotron Light Facility, 08290 Barcelona, Spain*

Complete contact information is available at: https://pubs.acs.org/10.1021/acs.jpcc.2c01184


### Author Contributions

The manuscript was written through the contributions of all authors. All authors have given approval to the final version of the manuscript.

### Notes

The authors declare no competing financial interest.

The data that support the findings of this study are available from the corresponding author upon reasonable request.

## ACKNOWLEDGMENTS

The authors acknowledge financial support from the Spanish Research Agency (AEI) and the Spanish Ministry of Science and Investigation (MCIN) under grant PID2019106383GB-C41 (DOI: 10.13039/501100011033) and by the Generalitat Valenciana under grant no. Prometeo/2018/123 (EFIMAT). J.S-M. acknowledges the Spanish Ministry of Science, Innovation and Universities for the PRE2020-092198 predoctoral fellowship. The authors thank ALBA synchrotron for providing beam time for the XRD experiments (Proposals 2015081344 and 2016081779).

## REFERENCES


(1) He, R. a.; Cao, S.; Zhou, P.; Yu, J. Recent Advances in Visible Light Bi-based Photocatalysts. *Chin. J. Catal.* **2014**, *35*, 989−1007.

(2) Kudo, A.; Miseki, Y. Heterogeneous Photocatalyst Materials for Water Splitting. *Chem. Soc. Rev.* **2009**, *38*, 253−278.

(3) Iwase, A.; Ng, Y. H.; Ishiguro, Y.; Kudo, A.; Amal, R. Reduced Graphene Oxide as a Solid-State Electron Mediator in Z-Scheme Photocatalytic Water Splitting under Visible Light. *J. Am. Chem. Soc.* **2011**, *133*, 11054−11057.

(4) Hazen, R. M.; Mariathasan, J. W. E. Bismuth Vanadate: A High-Pressure, High-Temperature Crystallographic Study of the Ferroelastic-Paraelastic Transition. *Science* **1982**, *216*, 991.

(5) Parmar, K. P. S.; Kang, H. J.; Bist, A.; Dua, P.; Jang, J. S.; Lee, J. S. Photocatalytic and Photoelectrochemical Water Oxidation over Metal-Doped Monoclinic $BiVO_4$ Photoanodes. *ChemSusChem* **2012**, *5*, 1926−1934.
(6) Errandonea, D.; Garg, A. B.; Pellicer-Porres, J.; Martinez-Garcia, D.; Popescu, C. Monoclinic-Tetragonal-Monoclinic Phase Transitions in $Eu_{0.1}Bi_{0.9}VO_4$ Under Pressure. *J. Phys.: Condens. Matter* **2019**, *31*, 485401.
(7) Dong, X.; Huangfu, Z.; Liang, Y.; Yuan, C.; Li, S.; Zhu, X.; Jiang, L.; Yang, K.; Wang, Y.; Cheng, X.; et al. Increasing Doping Solubility of $RE^{3+}$ Ions in Fergusonite $BiVO_4$ via Pressure-Induced Phase Transition. *J. Phys. Chem. C* **2021**, *125*, 22388−22395.
(8) Errandonea, D.; Garg, A. B. Recent Progress on the Characterization of the High-Pressure Behaviour of $AVO_4$ Orthovanadates. *Prog. Mater. Sci.* **2018**, *97*, 123−169.
(9) Bierlein, J. D.; Sleight, A. W. Ferroelasticity in $BiVO_4$. *Solid State Commun.* **1975**, *16*, 69−70.
(10) Sleight, A. W.; Chen, H.-y.; Ferretti, A.; Cox, D. E. Crystal Growth and Structure of $BiVO_4$. *Mater. Res. Bull.* **1979**, *14*, 1571−1581.
(11) Dreyer, G.; Tillmanns, E. Dreyerite: ein Naturliches, Tetragonales Wismutvanadat von Hirschhorn/Pfalz. *Neues Jahrb. Mineral. Monatsh.* **1981**, *1981*, 151−154.
(12) Qurashi, M. M.; Barnes, W. H. The Structure of Pucherite, $BiVO_4$. *Am. Mineral.* **1953**, *38*, 489−500.
(13) Pinczuk, A.; Welber, B.; Dacol, F. H. Mechanism of the Ferroelastic Transition of $BiVO_4$. *Solid State Commun.* **1979**, *29*, 515−518.
(14) Wood, I. G.; Welber, B.; David, W. I. F.; Glazer, A. M. Role of the Ferroelastic Strain in the Optical Absorption of $BiVO_4$. *J. Appl. Cryst.* **1980**, *13*, 224−229.
(15) Errandonea, D. Landau Theory Applied to Phase Transitions in Calcium Orthotungstate and Isostructural Compounds. *Europhys. Lett.* **2007**, *77*, 56001.
(16) Pellicer-Porres, J.; Vázquez-Socorro, D.; López-Moreno, S.; Muñoz, A.; Rodríguez-Hernández, P.; Martínez-García, D.; Achary, S. N.; Rettie, A. J. E.; Mullins, C. B. Phase Transition Systematics in $BiVO_4$ by Means of High-Pressure−High-Temperature Raman Experiments. *Phys. Rev. B* **2018**, *98*, 214109.
(17) Cheng, X.; Guan, J.; Jiang, L.; Zhang, H.; Wang, P.; Adeniyi, A. O.; Yao, Y.; Su, L.; Song, Y. Pressure-induced Structural Transformations and New Polymorphs in $BiVO_4$. *Phys. Chem. Chem. Phys.* **2020**, *22*, 10238−10246.
(18) Errandonea, D.; Meng, Y.; Somayazulu, M.; Häusermann, D. Pressure-Induced $\alpha \rightarrow \omega$ Transition in Titanium Metal: a Systematic Study of the Effects of Uniaxial Stress. *Phys. B* **2005**, *355*, 116−125.
(19) Gomis, O.; Sans, J. A.; Lacomba-Perales, R.; Errandonea, D.; Meng, Y.; Chervin, J. C.; Polian, A. Complex High-Pressure Polymorphism of Barium Tungstate. *Phys. Rev. B* **2012**, *86*, 054121.
(20) Garg, A. B.; Errandonea, D.; Rodríguez-Hernández, P.; Muñoz, A. High-Pressure Monoclinic−Monoclinic Transition in Fergusonite-type $HoNbO_4$. *J. Phys.: Condens. Matter* **2021**, *33*, 195401.
(21) Garg, A. B.; Rao, R.; Errandonea, D.; Pellicer-Porres, J.; Martinez-Garcia, D.; Popescu, C. Pressure-Induced Instability of the Fergusonite Phase of $EuNbO_4$ Studied by in situ Raman Spectroscopy, X-ray Diffraction and Photoluminescence Spectroscopy. *J. Appl. Phys.* **2020**, *127*, 175905.
(22) Marqueño, T.; Errandonea, D.; Pellicer-Porres, J.; Martinez-Garcia, D.; Santamaria-Pérez, D.; Muñoz, A.; Rodríguez-Hernández, P.; Mujica, A.; Radescu, S.; Achary, S. N.; et al. High-Pressure Polymorphs of Gadolinium Orthovanadate: X-ray Diffraction, Raman Spectroscopy, and Ab Initio Calculations. *Phys. Rev. B* **2019**, *100*, 064106.
(23) Bhattacharya, A. K.; Mallick, K. K.; Hartridge, A. Phase Transition in $BiVO_4$. *Mater. Lett.* **1997**, *30*, 7−13.
(24) Klotz, S.; Chervin, J.-C.; Munsch, P.; Le Marchand, G. Hydrostatic Limits of 11 Pressure Transmitting Media. *J. Phys. D Appl. Phys.* **2009**, *42*, 075413.
(25) Chijioke, A. D.; Nellis, W. J.; Soldatov, A.; Silvera, I. F. The Ruby Pressure Standard to 150 GPa. *J. Appl. Phys.* **2005**, *98*, 114905.
(26) Dewaele, A.; Loubeyre, P.; Mezouar, M. Equations of State of Six Metals above 94 GPa. *Phys. Rev. B* **2004**, *70*, 094112.
(27) Datchi, F.; LeToullec, R.; Loubeyre, P. Improved Calibration of the $SrB_4O_7$:$Sm^{2+}$ Optical Pressure Gauge: Advantages at very High Pressures and High Temperatures. *J. Appl. Phys.* **1997**, *81*, 3333−3339.
(28) Kraus, W.; Nolze, G. POWDER CELL - a Program for the Representation and Manipulation of Crystal Structures and Calculation of the Resulting X-ray Powder Patterns. *J. Appl. Crystallogr.* **1996**, *29*, 301−303.
(29) Toby, B. H.; Von Dreele, R. B. GSAS-II: The Genesis of a Modern Open-Source all Purpose Crystallography Software Package. *J. Appl. Crystallogr.* **2013**, *46*, 544−549.
(30) Garg, A. B.; Errandonea, D.; Rodríguez-Hernández, P.; Muñoz, A. $ScVO_4$ under non-Hydrostatic Compression: A New Metastable Polymorph. *J. Phys.: Condens. Matter* **2016**, *29*, 055401.
(31) Knight, K. S. Analytical Expressions to Determine the Isothermal Compressibility Tensor and the Isobaric Thermal Expansion Tensor for Monoclinic Crystals: Application to Determine the Direction of Maximum Compressibility in Jadeite. *Phys. Chem. Miner.* **2010**, *37*, 529−533.
(32) Cliffe, M. J.; Goodwin, A. L. PASCal: a Principal Axis Strain Calculator for Thermal Expansion and Compressibility Determination. *J. Appl. Cryst.* **2012**, *45*, 1321−1329.
(33) Errandonea, D. High Pressure Crystal Structures of Orthovanadates and their Properties. *J. Appl. Phys.* **2020**, *128*, 040903.
(34) Birch, F. Finite Rlastic Strain of Cubic Crystals. *Phys. Rev.* **1947**, *71*, 809−824.
(35) Angel, R. J. Equations of State. *Rev. Mineral. Geochem.* **2000**, *41*, 35−59.
(36) Gonzalez-Platas, J.; Alvaro, M.; Nestola, F.; Angel, R. EosFit7-GUI: a New Graphical User Interface for Equation of State Calculations, Analyses and Teaching. *J. Appl. Cryst.* **2016**, *49*, 1377−1382.
(37) Farid Ul Islam, A.; Nurul Huda Liton, M.; Tariqul Islam, H.; Al Helal, M.; Kamruzzaman, M. Mechanical and Thermodynamical Stability of $BiVO_4$ Polymorphs Using First-Principles Study. *Chin. Phys. B* **2017**, *26*, 036301.
(38) Errandonea, D.; Boehler, R.; Japel, S.; Mezouar, M.; Benedetti, L. R. Structural Transformation of Compressed Solid Ar: An X-ray Diffraction Study to 114 GPa. *Phys. Rev. B* **2006**, *73*, 092106.
(39) Aizu, K. Determination of the State Parameters and Formulation of Spontaneous Strain for Ferroelastics. *J. Phys. Soc. Jpn.* **1970**, *28*, 706.
(40) Arulnesan, S. W.; Kayser, P.; Kimpton, J. A.; Kennedy, B. J. Studies of the Fergusonite to Scheelite Phase Transition in $LnNbO_4$ Orthoniobates. *J. Solid State Chem.* **2019**, *277*, 229−239.


https://doi.org/10.1021/acs.jpcc.2c01184
J. Phys. Chem. C 2022, 126, 7755−7763